Engineering the electronic and optical properties of 2D porphyrin paddlewheel metal-organic frameworks

Article

Published Version

It is advisable to refer to the publisher's version if you intend to cite from the work. See [Guidance on citing](#).

www.reading.ac.uk/centaur

CentAUR

Central Archive at the University of Reading

Reading's research outputs online

PAPER • OPEN ACCESS

Engineering the electronic and optical properties of 2D porphyrin-paddlewheel metal-organic frameworks

View the article online for updates and enhancements.

Journal of Physics: Energy

Engineering the electronic and optical properties of 2D porphyrin-paddlewheel metal-organic frameworks

Victor Posligua[1] , Dimpy Pandya[1], Alex Aziz[2] , Miguel Rivera[2], Rachel Crespo-Otero[2] , Said Hamad[3] and Ricardo Grau-Crespo[1,*]

1 Department of Chemistry, University of Reading, Whiteknights, Reading RG6 6DX, United Kingdom
2 School of Biological and Chemical Sciences, Queen Mary University of London, Mile End Road, London E1 4NS, United Kingdom
3 Department of Physical, Chemical and Natural Systems, Universidad Pablo de Olavide, Ctra.de Utrera km.1, Seville 41013, Spain
* Author to whom any correspondence should be addressed.

E-mail: r.grau-crespo@reading.ac.uk

Abstract

Metal-organic frameworks (MOFs) are promising photocatalytic materials due to their high surface area and tuneability of their electronic structure. We discuss here how to engineer the band structures and optical properties of a family of two-dimensional porphyrin-based MOFs, consisting of M-tetrakis(4-carboxyphenyl)porphyrin structures (M-TCPP, where M = Zn or Co) and metal (Co, Ni, Cu or Zn) paddlewheel clusters, with the aim of optimising their photocatalytic behaviour in solar fuel synthesis reactions (water-splitting and/or CO_2 reduction). Based on density functional theory (DFT) and time-dependent DFT simulations with a hybrid functional, we studied three types of composition/structural modifications: (a) varying the metal centre at the paddlewheel or at the porphyrin centre to modify the band alignment; (b) partially reducing the porphyrin unit to chlorin, which leads to stronger absorption of visible light; and (c) substituting the benzene bridging between the porphyrin and paddlewheel, by ethyne or butadiyne bridges, with the aim of modifying the linker to metal charge transfer behaviour. Our work offers new insights on how to improve the photocatalytic behaviour of porphyrin- and paddlewheel-based MOFs.

1. Introduction

Metal-organic frameworks (MOFs) are materials where metal atoms or clusters are connected via organic linkers to form rigid frameworks, often with a porous structure [1]. They have found applications in gas (e.g. CO_2, H_2) storage and separation [2–6]. More recently, MOFs have been investigated as potential photocatalysts due to their tuneable electronic and optical behaviour, as there is a huge compositional space of transition metal ions/clusters or multidentate organic linkers that can be incorporated into the framework [7–9]. Several strategies have been designed to modify MOFs for enhanced photocatalytic performance, including linker functionalization [10–12], mixing metals/linkers [13–16], and metal nanoparticle loading [17–20].

 Porphyrin-like organic units are particularly attractive as components of MOF photocatalysts, due to their remarkable light absorbing properties, which is also the basis of natural photosynthetic systems [21–23]. Several porphyrin-based MOFs have been investigated for photocatalysis. For example, Fateeva *et al* reported a water-stable porphyrin-based MOF with Al-carboxylate clusters as metal nodes, capable of performing photocatalytic production of hydrogen from water, in the presence of Pt nanoparticles [19]. A MOF consisting of Zn metalloporphyrins connected to Zr_6O_8 clusters through carboxylic groups, coupled with an organometallic $[Fe_2S_2]$ complex, has also shown photocatalytic activity for hydrogen evolution [24]. Leng *et al* [25] reported an indium-based porphyrinic MOF, USTC-8(In), where one-dimension In−oxo

chains are connected by the porphyrin units, with excellent photocatalytic H_2 production under visible light. In this system, the out-of-plane In^{3+} ions detach from the porphyrin ligands under excitation, avoiding the fast back electron transfer and thus electron–hole separation is improved. MOFs consisting of Ru_2 paddlewheel units and Zn-porphyrins were reported by Lan *et al* [26] to exhibit visible-light photocatalytic activity for hydrogen evolution, without the presence of metal co-catalysts. In that case, the proximity of the Ru cluster to the porphyrin ($\sim$11 Å) was found to facilitate the electron transfer from the photoexcited porphyrins to the metal clusters.

There has been recent interest in creating two-dimensional (2D) photocatalytic MOFs, which could benefit from very accessible active sites and short paths for the photogenerated charge carriers to reach the solid–water interface. Wang *et al* [20] have proposed ultrathin porphyrin-based MOFs consisting of Ti_7O_6 clusters and free-based porphyrins connected by H_2TCPP linkers, which exhibited excellent photocatalytic hydrogen evolution in the presence of Pt as co-catalyst. Porphyrin-based quasi-2D lanthanide MOFs with different thicknesses were synthesised by Jiang *et al* [27], demonstrating that the thinner materials had higher Brunauer–Emmett–Teller surface area, light harvesting ability, carrier density, separation efficiency, and therefore better photocatalytic performance.

Despite the remarkable progress in recent years, porphyrin-based MOFs still need efficiency improvement in the light absorption and charge separation processes to become viable photocatalysts. The optical behaviour of porphyrin-based MOFs is still not well understood at a fundamental level, which hinders the optimisation process. Computer simulations based on density functional theory (DFT) can be very useful in rationalising the electronic and optical properties of MOFs [28]. Previous DFT simulation work from our group [29, 30] on 3D porphyrin-based MOFs similar to those synthesised by Fateeva *et al* [19] has shown that the choice of metal at the porphyrin centre or at the metal clusters can be used to optimise the band alignment for the photocatalytic process. We showed that when Al cations in the porphyrin-based MOFs are replaced by Fe cations, the position of the conduction band edge is lowered significantly, and that the Fe/Al ratio in the mixed-metal MOF can be used to tune the band edge positions.

In this work, we investigate a class of 2D porphyrin-based MOFs consisting of *M*-tetrakis (4-carboxyphenyl)porphyrin structures (*M*-TCPP, where $M = Zn^{2+}$ or Co^{2+}) and metal paddlewheel clusters ($M_2(COO^-)_4$). It is known that the metal paddlewheel cluster structure can accommodate different metals, e.g. $M = Co^{2+}$, Ni^{2+}, Cu^{2+}, Zn^{2+}, Cd^{2+}, Mn^{2+} [31]. We consider here metal paddlewheels made of late $3d$ metals ($M = Co^{2+}$, Ni^{2+}, Cu^{2+}, or Zn^{2+}). The paddlewheel cluster comprises of two divalent metal ions bridged together by four carboxylate ligands. Each paddlewheel is then linked to four porphyrin units (figure 1). A MOF with this layer structure was synthesised by Choi *et al* [32] in bulk form, with layers exhibiting AB stacking. Zhao *et al* [33, 34] showed how to grow this material anisotropically, with the help of surfactants, to create 2D nanosheets with only 8 ± 3 layers. Spoerke *et al* [35] also reported the synthesis and characterisation of 2D structures consisting of Zn-paddlewheels and Zn-porphyrins and showed that these structures can serve as active components in photovoltaic systems.
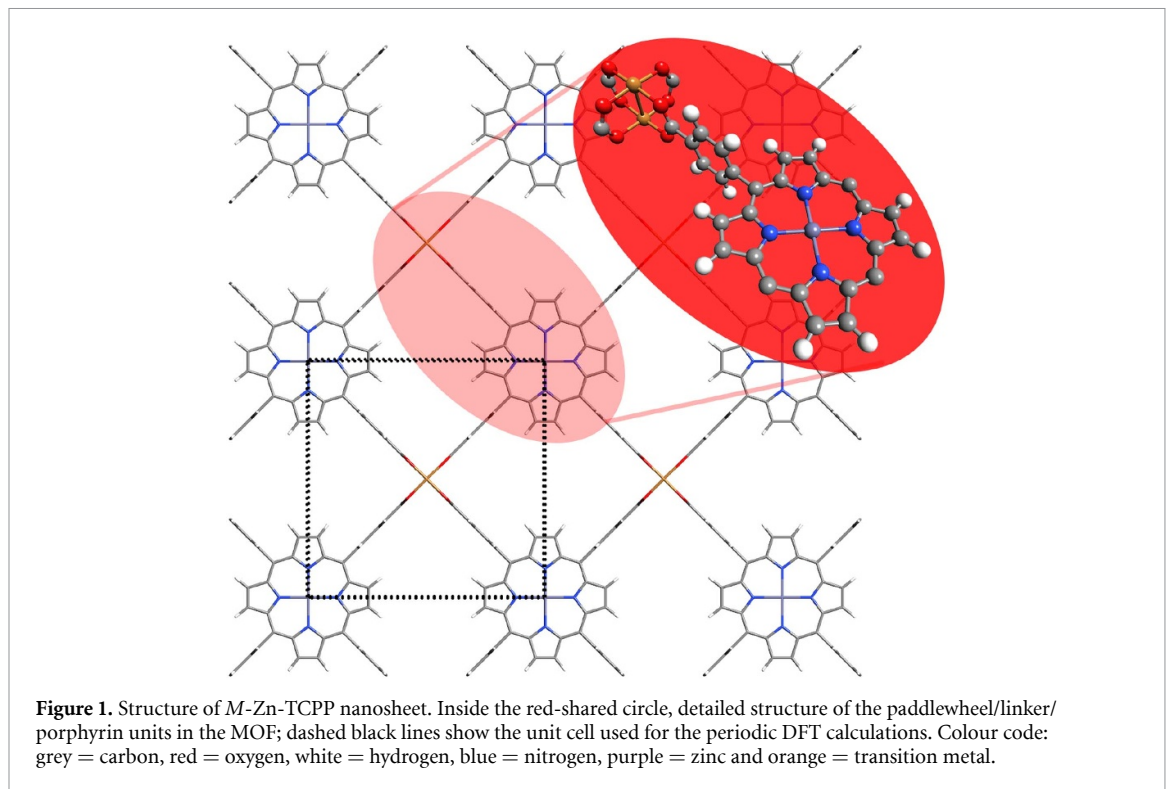
The presence of porphyrin in a 2D pattern, and the possibility of tuning the electronic properties by changing the paddlewheel metal, make this family of materials potentially interesting for photocatalysis. One possible concern is the poor hydrolytic stability of some metal paddlewheel frameworks [36, 37]. At harsh environments (i.e. high water loading), a hydrolysis reaction of water molecules with Cu–O–C groups can induce the structural decomposition of Cu paddlewheels [36]. However, the stability in water depends on the nature of the metal in the paddlewheel and on the water loading [38, 39] which means that some of the 2D-MOFs investigated here could still be useful as photocatalysts. They are also promising in other applications (e.g. as photovoltaic materials), where the electronic properties are of interest.

Due to their simplicity, these 2D-MOFs provide useful model systems to investigate how to engineer the electronic and optical behaviour of porphyrin-based MOFs. The aim of this paper is to investigate how different modifications (change in metal centres, functionalization of the porphyrins, or changes in the organic bridge between the porphyrin and the paddlewheel) can tune the electronic and optical properties of 2D porphyrin-paddlewheel MOFs for photocatalytic and other applications.

2. Methodology

Calculations of the periodic models were performed using DFT as implemented in the VASP program [40, 41]. The simulation cell consists of one Zn^{2+} centred porphyrin linker and one metal paddlewheel node (figure 1). Vacuum regions separating the layers from their periodic images have a width of $\sim$20 Å.

Two exchange-correlation functionals were employed. First, for the geometry optimisation of the ionic positions and lattice constants we used the computationally inexpensive generalised gradient approximation (GGA) with Perdew–Burke–Ernzerhof (PBE) [42, 43] exchange-correlation functional. Hubbard corrections were applied (PBE + U) to improve the poor description by the GGA of the highly-localised d orbitals of the

Figure 1. Structure of *M*-Zn-TCPP nanosheet. Inside the red-shared circle, detailed structure of the paddlewheel/linker/porphyrin units in the MOF; dashed black lines show the unit cell used for the periodic DFT calculations. Colour code: grey = carbon, red = oxygen, white = hydrogen, blue = nitrogen, purple = zinc and orange = transition metal.

transition metal atoms [44]. We used U_{eff} values of 3.3, 4.0 and 6.4 eV for Co, Cu and Ni, respectively [45]. Grimme's empirical corrections were also used, to account for long-range dispersion effects that are not well described by the GGA [46]. A Γ-centred *k*-grid of 4 × 4 × 1 *k*-points (six irreducible reciprocal lattice points) was used for these relaxation calculations. During relaxation, the cell parameters were allowed to relax while keeping the cell volume constant, so that the vacuum gap was preserved. The forces on the atoms were minimised until they were less than 0.02 eV Å^{-1}.

The screened hybrid functional (HSE06) [47, 48] was then used for single-point calculations at the PBE + U equilibrium geometries, in order to obtain more accurate electronic structures and band gap values of the materials. The HSE06 functional, which mixes the PBE exchange with the exact exchange from Hartree–Fock theory, is known to predict accurate band gaps for a wide range of semiconducting solids [49]. For the HSE06 calculations, a reduced mesh of 2 × 2 × 1 *k*-point mesh was used to compensate for the higher computational cost of evaluating the exact exchange. Using a test case, we checked that our combined PBE + U/HSE06 approach gave results not significantly different from those obtained using HSE06 for both relaxation and electronic structure simulations, which is computationally much more demanding. From these calculations, we only extracted the band gaps and band alignment of the materials, but not full band structures, as the latter would involve considerably higher computational cost for the wide range of compositions in this study. However, it would be interesting in future work to investigate the full band structure of these materials to understand the carrier mobility within the frameworks, as recently done by García-Valdivia *et al* for another series of 2D MOFs [50].

The projector augmented wave method [51, 52] was used to describe the interaction between the frozen core electrons (i.e. up to 3*p* for Ni, Cu, Zn and up to 1*s* for C, N, O) and its valence electrons and a kinetic energy cut-off of 400 eV was fixed for the plane-wave basis set expansion. All calculations were spin-polarised and we considered all possible spin states and relative orientations of the magnetic moments for the transition metal ions. For Cu^{2+} (d^9), only one spin state is possible, with one unpaired electron. For Ni^{2+} (d^8), two spin states are possible where there can be zero or two unpaired electrons, which correspond to low-spin (LS) or high-spin (HS), respectively. In the case of Co^{2+} (d^7), two spin states are possible also where there can be one or three unpaired electrons (LS and HS, respectively). For the spin-polarised ions, both antiferromagnetic (AFM) and ferromagnetic (FM) configurations were considered.

All the electron energies are reported with respect to the vacuum reference. As in other periodic DFT codes, the band energies in VASP are given with respect to an internal energy reference. Therefore, to obtain absolute energy levels it is necessary to evaluate the electrostatic potential in the pseudo-vacuum region represented by an empty space within the simulation cell, with zero potential gradient. This is chosen here as

Table 1. Relative stability and geometric parameters for different spin states and magnetic configurations of the 2D frameworks at each paddlewheel composition. μ is the local magnetic moment on each metal atom. $d[M\text{-}M]$ is the distance between the metal atoms in the paddlewheel. Energies are obtained from HSE calculations at PBE + U geometries. Values in bold indicate the calculated groundstate for each composition.

M	Spin state	μ (μ_B)	Magnetic configuration	Relative stability (eV)	a (Å)	d ($M\text{-}M$) (Å)
Co(II)	**HS**	**3**	AFM	+0.25	16.75	2.45
			FM	**0**	**16.74**	**2.53**
	LS	1	AFM	+0.50	16.65	2.34
			FM	+0.69	16.63	2.36
Ni(II)	HS	2	AFM	+1.23	16.68	2.44
			FM	+0.43	16.71	2.58
	LS	**0**	—	**0**	**16.60**	**2.38**
Cu(II)	—	**1**	**AFM**	**0**	**16.73**	**2.45**
			FM	+0.03	16.70	2.45
Zn(II)	—	**0**	—	—	**16.80**	2.55

the planar average in the middle of the vacuum gap between the nanosheets. The MacroDensity code was employed for this purpose [53].

Finally, using the Gaussian16 code [54], time-dependent DFT calculations (TD-DFT) were also performed in order to examine the excited states in some selected cases. For these calculations, the MOF systems were represented by cluster models consisting of one porphyrin and one paddlewheel unit, where all the cleaved C bonds were saturated with H atoms (figures S3–S5 in the SI (available online at stacks.iop.org/JPENERGY/3/034005/mmedia)). The geometries of the clusters were fixed to those obtained from the periodic calculations. For consistency, we used the same HSE06 functional as in the VASP calculations. Triplet states were used to describe the magnetic nature of the copper paddlewheel clusters. The calculations were all-electron (i.e. no pseudopotentials were employed) and a 6–311G(d,p) basis set was used to expand the wavefunctions.

3. Results and discussion

3.1. Framework geometry and magnetic ground states

We first discuss how the nature of the paddlewheel metal affects the geometric and electronic properties of the framework. Table 1 summarises the relative stabilities and geometric parameters of the frameworks with different paddlewheel compositions (Co, Ni, Cu or Zn), spin state and magnetic ordering. The metal at the centre of the porphyrin was kept as Zn in all cases.

Except in the case of the non-magnetic Zn^{2+} cations, we need to investigate different spin states and magnetic ordering for each paddlewheel composition. We only consider initial magnetic moments corresponding to spin states compatible with the +2 oxidation state of each metal centre, as this is the expected oxidation state of the metal atoms in paddlewheel units (to compensate the charges of the four COO^- groups). We checked in each case that the final local magnetic moments and magnetisation after relaxation were still consistent with the initial spin configurations. The Cu paddlewheel exhibits AFM coupling between the two neighbouring metal centres in the paddlewheel, which is consistent with both experimental measurements in Cu paddlewheel clusters [55–57] and with the theoretical study by Rodriguez-Fortea *et al* [58]. For Co, the preferred spin state of each metal cation is HS, which involves a local magnetic moment $\mu = 3\ \mu_B$ per Co(II) cation. This result agrees with the experimental determination by Pakula and Berry, who showed that Co(II) species are in HS state in Co paddlewheel units [59], although they found that the local magnetic moments were aligned antiferromagnetically within the paddlewheel, whereas in our calculation we found that the FM alignment is more stable.

For the Ni case, our calculations give the LS state as the ground state, contrasting with the experimental measurements by Pang *et al* [56] who found an HS AFM ground state in Ni paddlewheel clusters. In general, the comparison between theoretically and experimentally determined electronic ground states is difficult for these systems, because our calculations refer to systems with coordinatively unsaturated metal centres, i.e. only the four equatorial carboxylate ligands are considered, whereas in most experimental situations the metal centres in the paddlewheel are saturated by additional linkers or solvent molecules, e.g. water [56] or ethanol [59]. If we perform our calculation for the Ni-paddlewheel system with water molecules added in axial position making each Ni centre penta-coordinated, then we find that the HSAFM state is the most stable, followed by the HS ferromagnetic ground state, which in this case is only 0.06 eV higher in energy. In any case, we have found that the band alignment presented below does not change much with the nature of
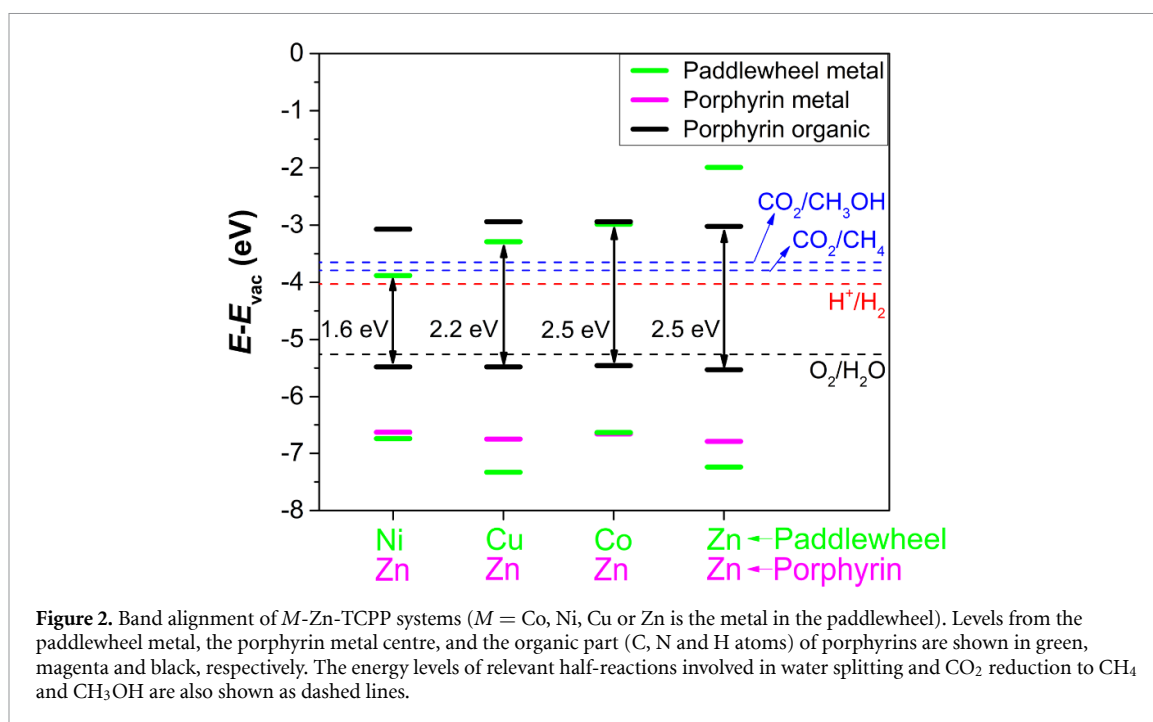
Figure 2. Band alignment of *M*-Zn-TCPP systems (*M* = Co, Ni, Cu or Zn is the metal in the paddlewheel). Levels from the paddlewheel metal, the porphyrin metal centre, and the organic part (C, N and H atoms) of porphyrins are shown in green, magenta and black, respectively. The energy levels of relevant half-reactions involved in water splitting and CO_2 reduction to CH_4 and CH_3OH are also shown as dashed lines.

the magnetic ground state. The results presented below refer to the magnetic ground states found theoretically in this work for the paddlewheel units with tetra-coordinated metal centres.

The cell parameter of the Zn-paddlewheel framework (16.80 Å) can be compared with the experimental value obtained by x-ray diffraction for stacked 2D porphyrin-paddlewheel nanosheets with the same composition, which was 16.71 Å [60]. The discrepancy (0.5%) is small considering the approximations in the DFT simulation, related to both the limitations of the exchange-correlation functional and to ignoring vibrational effects. Furthermore, the experimental value refers to the bulk material, whereas the simulation corresponds to a single-layer material. The variation of both the cell parameter and the *M-M* distance is consistent with the trend of ionic radii for Co^{2+}, Ni^{2+}, Cu^{2+} and Zn^{2+}, which is not monotonous along the period but has a minimum value for Ni^{2+} [61].

3.2. Effect of changing the paddlewheel metal on the band positioning

We now discuss the suitability of the band structure alignment for the photocatalysis of solar fuel synthesis from H_2O or CO_2, as a function of the nature of the metal in the paddlewheel. For this analysis, we need to align the band edges with respect to the vacuum potential, to obtain their absolute positions, and compare with the redox potentials for the photocatalytic reaction. The valence and conduction bands must straddle the redox potentials for the given reaction. For example, for water-splitting, the valence band edge should be below the energy of the oxygen evolution reaction (OER):

$$H_2O \leftrightarrow 2H^+_{(aq)} + \tfrac{1}{2}O_{2(g)} + 2e^- \tag{1}$$

while the conduction band edge should be above the energy of the hydrogen evolution reaction (HER):

$$2H^+_{(aq)} + 2e^- \leftrightarrow H_{2(g)}. \tag{2}$$

The difference between these redox potentials is 1.23 eV and therefore the band gap needs to be higher than this value. The optimal band gap for water-splitting is ∼2 eV [62] to take into consideration loss mechanisms, i.e. via thermal energy. At pH = 0 in the vacuum scale, the potential value for OER is −5.67 eV and for HER is −4.44 eV. These potentials are shifted by $k_B T \times pH \times \ln 10$ (where k_B is Boltzmann's constant) for systems at finite temperature T and pH. The redox potentials values for water splitting at a neutral pH and room temperature are −5.26 eV and −4.03 eV for OER (O_2/H_2O) and HER (H^+/H_2), respectively. For CO_2 reduction the band edges must straddle a larger redox potential difference, with carbon dioxide reduction to methane (CO_2/CH_4) at −3.79 eV and carbon dioxide reduction to methanol (CO_2/CH_3OH) at −3.65 eV. All these potentials and the positions of the band edges and band gaps are shown in figure 2.

It is shown that the valence band, which is mainly contributed by the porphyrin unit, is approximately at −5.5 eV, which is below the OER, as required. The nature of the paddlewheel metal mainly affects the
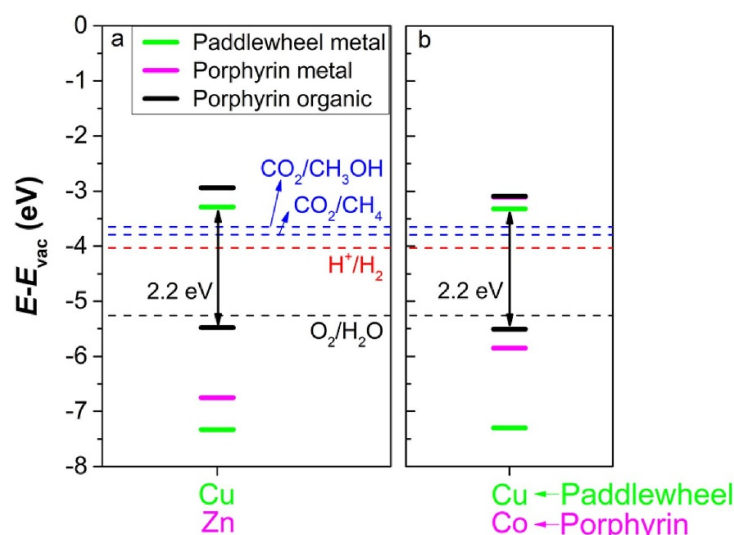
Figure 3. Comparison between band alignments of (a) Cu–Zn-TCPP and (b) Cu–Co-TCPP systems. The energy levels of the metal at paddlewheel, the metal at the porphyrin centre and organic part (C, N and H atoms) of porphyrins are shown in green, magenta and black, respectively. The energy levels of relevant half-reactions involved in water splitting and CO_2 reduction to CH_4 and CH_3OH are also shown as dashed lines.

position of the conduction band edge. Whereas the lowest unoccupied molecular orbital (LUMO) of the porphyrin is always at the same energy ($\sim$ −3 eV), the empty $3d$ levels of the paddlewheel transition metal centres can go below that value, lowering the band gap. For the Ni–Zn system, a lower-lying, empty Ni $3d$ level narrows the band gap to 1.6 eV, where in the Co–Zn system, the lowest empty Co $3d$ level is at the same energy as the porphyrin's LUMO, so the band gap is not narrowed. For water-splitting photocatalysis, the best metal in the paddlewheel is Cu, whose empty $3d$ levels bring the band gap to 2.2 eV. The Co–Zn system also has suitable band positions, albeit with a larger gap, which might be useful for photocatalytic CO_2 reduction reactions.

Taking the Cu–Zn system as reference, we can form a picture of how the photocatalytic water-splitting reaction could occur in a system like this. A water molecule would interact with the porphyrin unit (we have calculated an adsorption energy of −0.26 eV for water at the Zn-porphyrin in this MOF), where a photogenerated hole would drive the water oxidation reaction, evolving oxygen gas. A ligand-to-metal charge transfer (LMCT) would then have to take place, moving the excited electron from the excited levels of the porphyrin to the metal paddlewheel, where the reduction of protons would occur, driven by the high energy of the excited electron in the Cu $3d$ state.

TD-DFT calculations in a cluster model of the Cu–Zn-TCPP system confirm that the lowest-energy electronic excitation (T_1) involves charge transfer (CT) from the porphyrin to the paddlewheel (see SI: table S1 for the list of excited states and table S2 for the relative charges of the porphyrin and paddlewheel units). However, this first excitation has zero oscillator strength, i.e. the CT cannot be achieved via direct excitation. The lowest bright excitation (T_{44}) is a transition localized within the porphyrin unit, and corresponds to the so-called Soret band (or B band) of the porphyrin, which typically appears in the far visible or ultraviolet (UV) region of the spectrum [21, 63–65]. These calculations suggest two limitations of these porphyrin-based MOFs in photocatalytic applications. First, most of the adsorption happens at energies in the far visible or UV range of the spectrum, so it would not be possible to take advantage of most of the energy from solar radiation, which lies in the visible region. Second, since the oscillator strength of the CT state is very low, we need to engineer the structure to make CT more feasible. Therefore, in the next sections we will consider possible modifications to these MOFs, which could enhance their photocatalytic properties.

3.3. Effect of changing the metal from Zn to Co at the porphyrin centre
We now briefly consider the substitution of Zn by Co at the porphyrin centre, for which we have investigated the band positions in a system with Co at the centre of the porphyrin and Cu in the paddlewheel. The conduction band for this Cu–Co system is 0.3 eV below the LUMO of the porphyrin, which is similar to what is observed for the Cu–Zn system (figure 3).

However, the highest filled $3d$ levels of the Co centres are significantly higher in energy than the highest filled $3d$ levels of Zn. The proximity between the high-lying filled Co $3d$ levels and the highest-occupied molecular orbital level of the porphyrin will help stabilize a photogenerated hole, since the Co(II) centre can
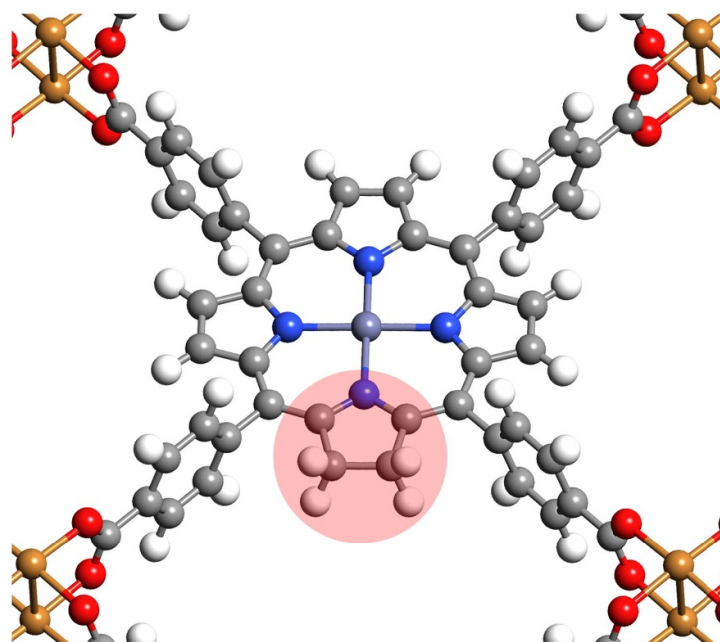
Figure 4. The Cu-Zn-chlorin system: the C_β atoms of the pink-shaded pyrrole are reduced. Colour code: grey = carbon, red = oxygen, white = hydrogen, blue = nitrogen, orange = copper.

be readily oxidised to Co(III) (in contrast with the case of Zn, whose low-lying filled $3d$ levels prevent the oxidation). The presence of Co as a redox centre in porphyrins has been widely used in the experimental design of porphyrin-based photocatalysts [66, 67].

Although Co-porphyrins seem more interesting for photocatalysis than Zn-porphyrins, in what follows we will consider other modifications of the porphyrin-based MOFs, while keeping the Zn at the porphyrin centre, for ease of calculations (the Co centres introduce additional magnetic degrees of freedom). The effect of other metal centres at the porphyrin on the electronic structure of porphyrin-based MOFs has been investigated in more detail in [29].

3.4. Effect of partially reducing the porphyrin unit to chlorin

Until this point, we have explored substitutions of the metals at the paddlewheel and porphyrin units. Another route to modify the electronic properties and optical behaviour of these MOFs is to partially reduce the porphyrin unit to form chlorin. Chlorins fall in the generic class of hydroporphyrins, that is, porphyrin derivatives in which one or more bonds are saturated by addition of hydrogen, resembling a photosynthetic chromophore found in nature [68]. It is known that chlorin exhibits stronger light absorption at lower energies compared to porphyrin [69]. Lu *et al* have successfully synthesised chlorin-based MOFs that improve the photophysical properties of porphyrin-based MOFs for photodynamic therapy of colon cancers [70]. The motivation here is to study the increase of the light absorption of the MOF in the visible range to improve its photocatalytic efficiency.

The Cu-Zn-TCPP system was used as starting point, where one of the pyrrole rings was reduced by hydrogenation, as shown in figure 4. After optimisation, this system exhibited negligible changes of cell parameters and geometry compared to the Cu–Zn-TCPP one. In this structure, because of the application of periodic boundary conditions, the position of the reduced pyrrole is ordered. However, using a $2 \times 2 \times 1$ supercell, we have considered different relative positions of the reduced pyrrole in neighbouring chlorin units, and found that all configurations have similar energies (within 0.1 meV) and band gaps (within 0.05 eV). Therefore, our analysis below refers to the ordered configuration represented by a single unit cell.

The partial reduction leads to a narrower band gap (1.9 eV), but otherwise the electronic structure is similar to that of the unreduced Cu–Zn-TCPP system (figure 5). Although the valence band is now slightly above the OER level, it is possible in practical applications to realign such small differences using a bias voltage [29, 30].

Excited states calculations were performed for these Cu–Zn-chlorin systems (energies of all calculated states and Bader charges of selected states are listed in tables S3 and S4 of the SI). The first excited state (T_1), as in the unmodified porphyrin system, is a CT state, but with zero oscillator strength. The Soret band is also found at roughly the same energy in the porphyrin- and chlorin-based MOFs. However, the chlorin-based
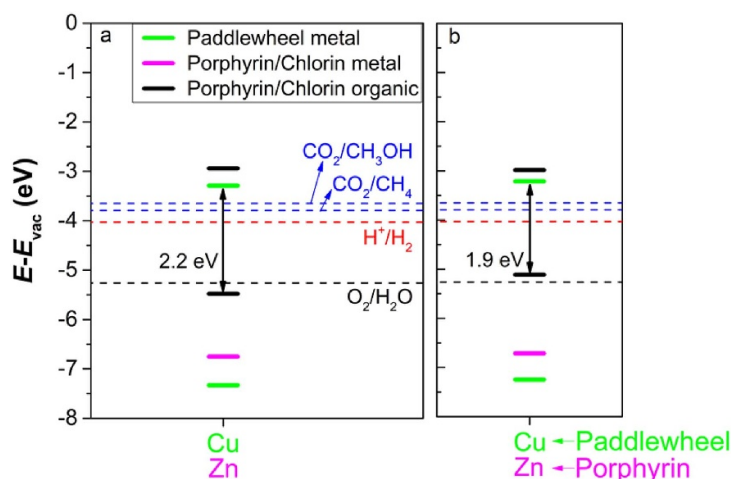
Figure 5. Comparison between band alignments of (a) Cu–Zn-TCPP and (b) Cu–Zn-chlorin systems. The bands of metal at paddlewheel, metal at the centre and organic part (C, N and H atoms of porphyrins) are shown in green, magenta and black, respectively. The energy levels of relevant half-reactions involved in water splitting and CO_2 reduction to CH_4 and CH_3OH are also shown as dashed lines.
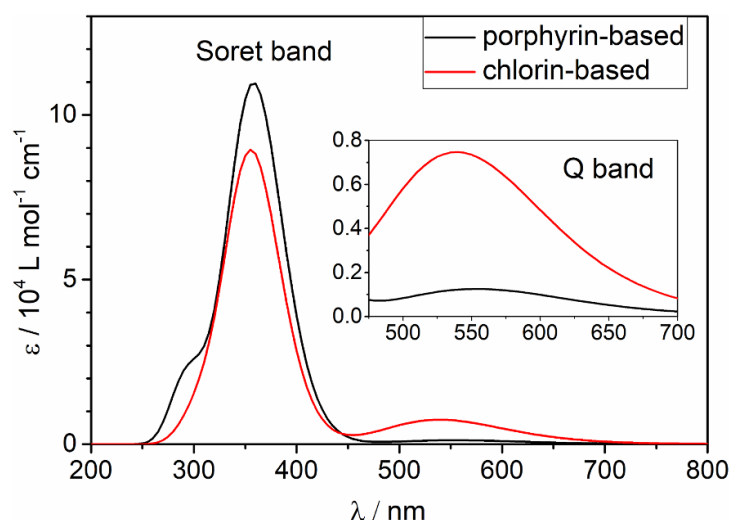

Figure 6. Light absorption spectra calculated using TD-DFT for the cluster models of the porphyrin-based (Cu–Zn-TCPP) and chlorin-based (Cu–Zn–chlorin) systems. The inset expands the spectrum in the region of the Q band.

MOF has a relatively bright state at lower energies (T_{16} at 2.3 eV) which is not present in the porphyrin-based system. This is consistent with previous work showing that chlorin increases light absorption in the lower-energy Q bands, thus improving photophysical behaviour under visible light [69, 70]. This is clearly observed in the absorption spectra of the cluster model of the Cu–Zn–chlorin system (figure 6), which shows the presence of a peak in the visible range. This peak corresponds to the Q bands, which in the case of the unreduced Cu–Zn-TCPP system is still appreciable but it has a very small intensity.

All these results suggest that the partial reduction of porphyrin to chlorin units in these and other MOFs could enhance the photocatalytic performance under visible light, but to the best of our knowledge this avenue has not been experimentally explored.

3.5. Changing the bridge between the porphyrin and paddlewheel

Finally, we consider the effect of modifying the bridging species between the porphyrin and the paddlewheel units. We investigate the substitution of the benzene rings by ethyne (C2) or butadiyne (C4) bridges (figure 7). We have shown in previous work that it is possible to modify the properties of porphyrin-based structures by varying the nature of the bridging species linking the porphyrins, and in this way tune the band gap values [71].
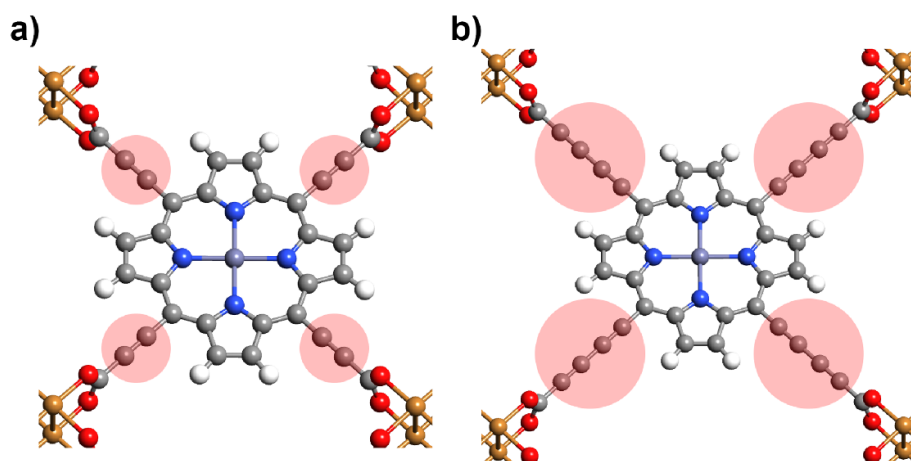
Figure 7. The two bridge-substituted systems studied in this work: (a) Cu–Zn-C2 and (b) Cu–Zn-C4. The benzene rings have been substituted by the ethyne and butadiyne bridges, respectively, highlighted by pink-shaded circles. Colour code: grey = carbon, red = oxygen, white = hydrogen, blue = nitrogen, orange = copper.
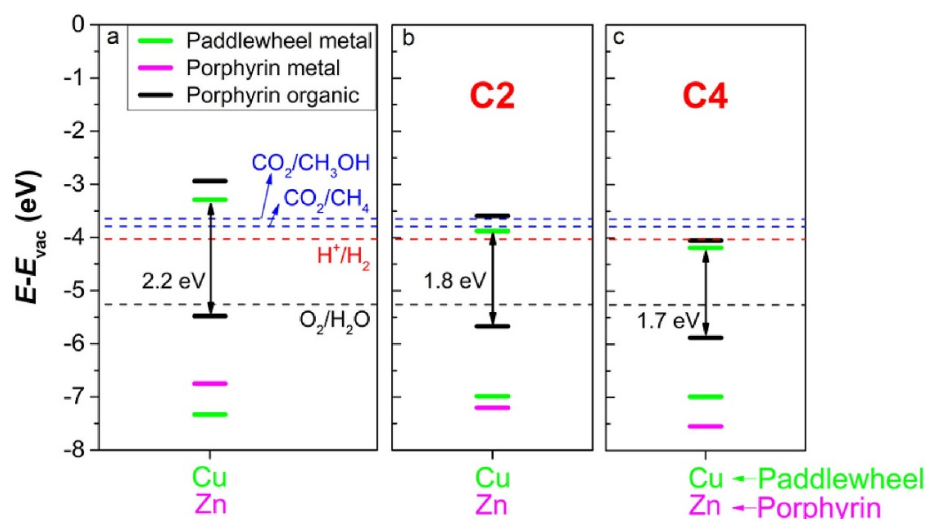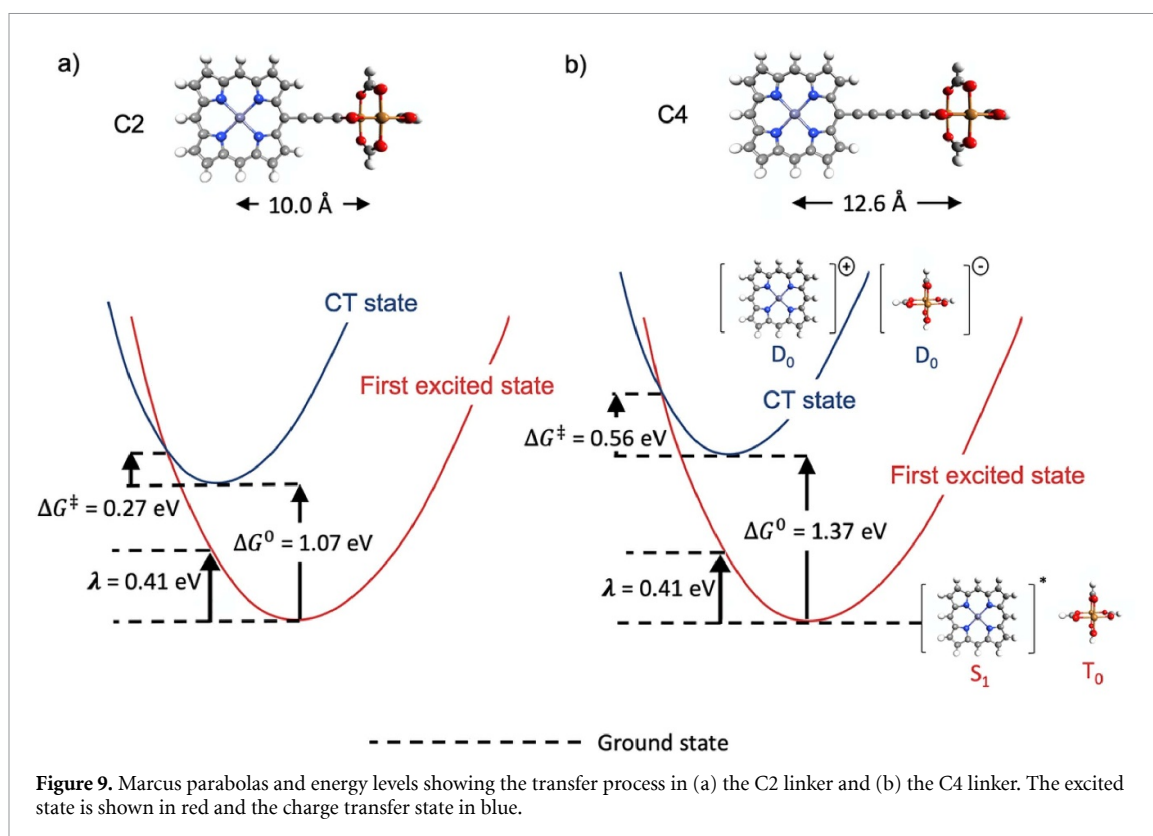

Figure 8. Comparison between band alignments of Cu–Zn-TCPP (left), Cu–Zn-C2 (middle) and -C4 (right) systems. The bands of metal at paddlewheel, metal at the centre and organic atoms of porphyrins (C, N and H) are shown in green, magenta and black, respectively. The energy levels of relevant half-reactions involved in water splitting and CO_2 reduction to CH_4 and CH_3OH are also shown.

The substitution of the benzene rings by C2 or C4 bridges induces significant narrowing of the band gaps (with values of 1.8 eV and 1.7 eV for C2 and C4, respectively) compared with the 2.2 eV value for the Cu–Zn-TCPP system (figure 8). The gap narrowing is achieved mainly as consequence of the lowering of the conduction bands, since the valence bands are almost unaltered, going only slightly down in energy.

It is interesting to discuss the effect of the different bridges on the charge transfer. The excited states for the system with the C2 bridge show that there are now several relatively bright states involving CT from the porphyrin to the paddlewheel (see tables S5 and S6 in the SI). Bright states T_{30}, T_{34} and T_{36}, which are at energies in the region of the Soret band, now involve significant CT from the porphyrin to the paddlewheel. This effect would lead to direct charge separation via light absorption and could potentially be beneficial for the photocatalytic behaviour of the system. Modifying the nature and length of the bridging units between the porphyrin and the metal cluster is thus the key to tune the CT behaviour.

The length of the bridging unit length can also be expected to modify the LMCT behaviour from excited states localized in the porphyrin. To illustrate this, we present here a simple model based on Marcus theory [72, 73], where we consider the porphyrin and the paddlewheel as two separate fragments. When light is absorbed at the bright states of the porphyrin, before any CT takes place, the excitation will decay to the first excited state of the porphyrin (Kasha's rule). We make use of Marcus theory to describe the electron transfer between the excited porphyrin fragment (donor) and the paddlewheel fragment (acceptor). To consider the

Figure 9. Marcus parabolas and energy levels showing the transfer process in (a) the C2 linker and (b) the C4 linker. The excited state is shown in red and the charge transfer state in blue.

electrostatic interaction between the charged fragments (porphyrin$^+$ and paddlewheel$^-$), we have simply added a classical electrostatic term to the energy of the CT state, considering the distance between these fragments (and assuming a full electron transfer).

In our model calculations, we find that the CT state is always above the first excited state, even at the equilibrium geometry of the CT state. The Marcus parabolas are positioned in figure 9 to reflect these relative energies. In this case, the barrier (with respect to the CT state) is given by $\Delta G^{\ddagger} = \left(\Delta G^0 - \lambda\right)^2/4\lambda$, where λ is the reorganization energy (defined here as the change in energy of the first excited state when moved to the geometry of the CT state, which in this simple model is independent of the length of the bridging unit). The energy of the charge-transfer state, and then the value of ΔG^0, is 0.3 eV lower for the C2 linker than that for the C4 linker, due to the stronger electrostatic attraction for the shorter bridge. This means that in the C2 system the kinetic barrier to go from one state to the other will also be lower, as shown in figure 9. Our analysis suggests that the introduction of shorter bridging units between the porphyrin and the metal clusters should lower the kinetic barriers for the LMCT process. This is consistent with the experimental work from Lan *et al* [26], who concluded that electron transfer from the photoexcited porphyrins to Ru clusters was facilitated by the proximity of the Ru cluster to the porphyrin in their MOF.

4. Conclusions

We have presented a computer simulation study of 2D, porphyrin(chlorin)-based MOFs, consisting of metalloporphyrin units (with Zn^{2+} or Co^{2+} at the centre) and metal paddlewheel clusters (made of Co^{2+}, Ni^{2+}, Cu^{2+} or Zn^{2+}), bridged by different organic linear chains. Our results illustrate several ways in which the electronic and optical properties of these MOFs can be modified by the different compositional or structural degrees of freedom. Changing the metal in the paddlewheel cluster from Zn to Co, Cu, or Ni, lowers the position of the empty 3*d* levels in that order. For Cu and Ni the empty 3d levels are slightly below the LUMO of the porphyrin, which is convenient to achieve charge separation via linker to metal CT. The copper paddlewheel seems ideal for water splitting photocatalysis in terms of the resulting band gap and relative position of empty levels. Changing the metal at the centre of the porphyrin from Zn to Co does not change of the band edges or the bandgap, but creates a flexible redox centre capable of stabilising the photogenerated hole at the porphyrin.

Perhaps even more important than engineering the band alignment and gap, is to enhance the visible light absorption and to facilitate charge separation in the framework. To address the first issue, we consider the partial reduction of porphyrin to chlorin in the MOF, which we demonstrate leads to stronger absorption

in the visible range of the spectrum. Charge separation, on the other hand, is found to be sensitive to the nature and length of the bridging units between the porphyrin and the paddlewheel. For example, using an ethyne bridge introduces charge-transfer bright states in the energy region of the Soret band. Finally, we used a simple model based on Marcus theory to illustrate that the energy barriers to the LMCT process can be expected to decrease with the length of the bridge. Overall, our study suggests different avenues to modify porphyrin-based MOFs to improve their photocatalytic performance in applications such as water splitting and CO_2 reduction.

Acknowledgments

ORCID iDs

Victor Posligua https://orcid.org/0000-0003-3375-3706
Alex Aziz https://orcid.org/0000-0002-6723-9871
Rachel Crespo-Otero https://orcid.org/0000-0002-8725-5350
Said Hamad https://orcid.org/0000-0003-4148-2344
Ricardo Grau-Crespo https://orcid.org/0000-0001-8845-1719

References

[1] Zhou H C, Long J R and Yaghi O M 2012 Introduction to metal–organic frameworks *Chem. Rev.* **112** 673–4
[2] Zhu G, Sun Q, Kawazoe Y and Jena P 2015 Porphyrin-based porous sheet: optoelectronic properties and hydrogen storage *Int. J. Hydrog. Energy* **40** 3689–96
[3] Ma S and Zhou H-C 2010 Gas storage in porous metal–organic frameworks for clean energy applications *Chem. Commun.* **46** 44–53
[4] Li B, Wen H-M, Zhou W and Chen B 2014 Porous metal–organic frameworks for gas storage and separation: what, how, and why? *J. Phys. Chem. Lett.* **5** 3468–79
[5] Li H, Wang K, Sun Y, Lollar C T, Li J and Zhou H-C 2018 Recent advances in gas storage and separation using metal–organic frameworks *Mater. Today* **21** 108–21
[6] Li H, Li L, Lin R-B, Zhou W, Zhang Z, Xiang S and Chen B 2019 Porous metal-organic frameworks for gas storage and separation: status and challenges *EnergyChem* **1** 100006
[7] Wang J-L, Wang C and Lin W 2012 Metal–organic frameworks for light harvesting and photocatalysis *ACS Catal.* **2** 2630–40
[8] Santaclara J G, Kapteijn F, Gascon J and Van Der Veen M A 2017 Understanding metal–organic frameworks for photocatalytic solar fuel production *CrystEngComm* **19** 4118–25
[9] Wang Q, Gao Q, Al-Enizi A M, Nafady A and Ma S 2020 Recent advances in MOF-based photocatalysis: environmental remediation under visible light *Inorg. Chem. Front.* **7** 300–39
[10] Fu Y, Sun D, Chen Y, Huang R, Ding Z, Fu X and Li Z 2012 An amine-functionalized titanium metal–organic framework photocatalyst with visible-light-induced activity for CO_2 reduction *Angew. Chem., Int. Ed.* **51** 3364–7
[11] Hendon C H, Tiana D, Fontecave M, Sanchez C, D'arras L, Sassoye C, Rozes L, Mellot-Draznieks C and Walsh A 2013 Engineering the optical response of the titanium-MIL-125 metal–organic framework through ligand functionalization *J. Am. Chem. Soc.* **135** 10942–5
[12] Hendrickx K, Vanpoucke D E, Leus K, Lejaeghere K, Van Yperen-De Deyne A, Van Speybroeck V, Van Der Voort P and Hemelsoet K 2015 Understanding intrinsic light absorption properties of UiO-66 frameworks: a combined theoretical and experimental study *Inorg. Chem.* **54** 10701–10
[13] Abednatanzi S, Derakhshandeh P G, Depauw H, Coudert F-X, Vrielinck H, Van Der Voort P and Leus K 2019 Mixed-metal metal–organic frameworks *Chem. Soc. Rev.* **48** 2535–65
[14] Li R, Ren X, Ma H, Feng X, Lin Z, Li X, Hu C and Wang B 2014 Nickel-substituted zeolitic imidazolate frameworks for time-resolved alcohol sensing and photocatalysis under visible light *J. Mater. Chem.* A **2** 5724–9
[15] Goh T W, Xiao C, Maligal-Ganesh R V, Li X and Huang W 2015 Utilizing mixed-linker zirconium based metal-organic frameworks to enhance the visible light photocatalytic oxidation of alcohol *Chem. Eng. Sci.* **124** 45–51
[16] Grau-Crespo R, Aziz A, Collins A W, Crespo-Otero R, Hernández N C, Rodriguez-Albelo L M, Ruiz-Salvador A R, Calero S and Hamad S 2016 Modelling a linker mix-and-match approach for controlling the optical excitation gaps and band alignment of zeolitic imidazolate frameworks *Angew. Chem., Int. Ed.* **55** 16012–6
[17] Yang Q, Xu Q and Jiang H-L 2017 Metal–organic frameworks meet metal nanoparticles: synergistic effect for enhanced catalysis *Chem. Soc. Rev.* **46** 4774–808

[18] Fang X, Shang Q, Wang Y, Jiao L, Yao T, Li Y, Zhang Q, Luo Y and Jiang H L 2018 Single Pt atoms confined into a metal–organic framework for efficient photocatalysis *Adv. Mater.* **30** 1705112

[19] Fateeva A, Chater P A, Ireland C P, Tahir A A, Khimyak Y Z, Wiper P V, Darwent J R and Rosseinsky M J 2012 A water-stable porphyrin-based metal–organic framework active for visible-light photocatalysis *Angew. Chem., Int. Ed.* **51** 7440–4

[20] Wang X, Zhang X, Zhou W, Liu L, Ye J and Wang D 2019 An ultrathin porphyrin-based metal-organic framework for efficient photocatalytic hydrogen evolution under visible light *Nano Energy* **62** 250–8

[21] Giovannetti R 2012 The use of spectrophotometry UV-vis for the study of porphyrins (*InTechOpen*)

[22] Lu Q, Yu Y, Ma Q, Chen B and Zhang H 2015 2D transition-metal-dichalcogenide-nanosheet-based composites for photocatalytic and electrocatalytic hydrogen evolution reactions *Adv. Mater.* **28** 1917–33

[23] Paschenko V Z, Konovalova N V, Bagdashkin A L, Gorokhov V V, Tusov V B and Yuzhakov V I 2012 Excitation energy transfer in covalently bonded porphyrin heterodimers *Opt. Spectrosc.* **112** 519–27

[24] Sasan K, Lin Q, Mao C and Feng P 2014 Incorporation of iron hydrogenase active sites into a highly stable metal–organic framework for photocatalytic hydrogen generation *Chem. Commun.* **50** 10390–3

[25] Leng F, Liu H, Ding M, Q-p L and Jiang H-L 2018 Boosting photocatalytic hydrogen production of porphyrinic MOFs: the metal location in metalloporphyrin matters *ACS Catal.* **8** 4583–90

[26] Lan G, Zhu Y-Y, Veroneau S S, Xu Z, Micheroni D and Lin W 2018 Electron injection from photoexcited metal–organic framework ligands to Ru$_2$ secondary building units for visible-light-driven hydrogen evolution *J. Am. Chem. Soc.* **140** 5326–9

[27] Jiang Z W, Zou Y C, Zhao T T, Zhen S J, Li Y F and Huang C Z 2020 Controllable synthesis of porphyrin-based 2D lanthanide metal–organic frameworks with thickness- and metal-node-dependent photocatalytic performance *Angew. Chem., Int. Ed.* **59** 3300–6

[28] Mancuso J L, Mroz A M, Le K N and Hendon C H 2020 Electronic structure modeling of metal–organic frameworks *Chem. Rev.* **120** 8641–715

[29] Hamad S, Hernandez N C, Aziz A, Ruiz-Salvador A R, Calero S and Grau-Crespo R 2015 Electronic structure of porphyrin-based metal–organic frameworks and their suitability for solar fuel production photocatalysis *J. Mater. Chem.* A **3** 23458–65

[30] Aziz A, Ruiz-Salvador A R, Hernández N C, Calero S, Hamad S and Grau-Crespo R 2017 Porphyrin-based metal-organic frameworks for solar fuel synthesis photocatalysis: band gap tuning via iron substitutions *J. Mater. Chem.* A **5** 11894–904

[31] Chung H, Barron P M, Novotny R W, Son H-T, Hu C and Choe W 2009 Structural variation in porphyrin pillared homologous series: influence of distinct coordination centers for pillars on framework topology *Cryst. Growth Des.* **9** 3327–32

[32] Choi E-Y, Wray C A, Hu C and Choe W 2009 Highly tunable metal–organic frameworks with open metal centers *CrystEngComm* **11** 553–5

[33] Zhao M, Lu Q, Ma Q and Zhang H 2017 Two-dimensional metal–organic framework nanosheets *Small Methods* **1** 1600030

[34] Zhao M *et al* 2015 Ultrathin 2D metal–organic framework nanosheets *Adv. Mater.* **27** 7372–8

[35] Spoerke E D, Small L J, Foster M E, Wheeler J, Ullman A M, Stavila V, Rodriguez M and Allendorf M D 2017 MOF-sensitized solar cells enabled by a pillared porphyrin framework *J. Phys. Chem.* C **121** 4816–24

[36] Tan K, Nijem N, Canepa P, Gong Q, Li J, Thonhauser T and Chabal Y J 2012 Stability and hydrolyzation of metal organic frameworks with paddle-wheel sbus upon hydration *Chem. Mater.* **24** 3153–67

[37] Chen Y, Wang B, Wang X, Xie L-H, Li J, Xie Y and Li J-R 2017 A copper(II)-paddlewheel metal–organic framework with exceptional hydrolytic stability and selective adsorption and detection ability of aniline in water *ACS Appl. Mater. Interfaces* **9** 27027–35

[38] Liu B, Vikrant K, Kim K-H, Kumar V and Kailasa S K 2020 Critical role of water stability in metal–organic frameworks and advanced modification strategies for the extension of their applicability *Environ. Sci.: Nano* **7** 1319–47

[39] Ding M, Cai X and Jiang H-L 2019 Improving MOF stability: approaches and applications *Chem. Sci.* **10** 10209–30

[40] Kresse G and Furthmüller J 1996 Efficient iterative schemes for *ab initio* total-energy calculations using a plane-wave basis set *Phys. Rev.* B **54** 11169–86

[41] Kresse G and Furthmüller J 1996 Efficiency of *ab-initio* total energy calculations for metals and semiconductors using a plane-wave basis set *Comput. Mater. Sci.* **6** 15–50

[42] Perdew J P, Burke K and Ernzerhof M 1996 Generalized gradient approximation made simple *Phys. Rev. Lett.* **77** 3865–8

[43] Perdew J P, Burke K and Ernzerhof M 1997 Generalized gradient approximation made simple [Phys. Rev. Lett. 77, 3865 (1996)] *Phys. Rev. Lett.* **78** 1396

[44] Dudarev S, Botton G, Savrasov S, Humphreys C and Sutton A 1998 Electron-energy-loss spectra and the structural stability of nickel oxide: an LSDA+ U study *Phys. Rev.* B **57** 1505

[45] Wang L, Maxisch T and Ceder G 2006 Oxidation energies of transition metal oxides within the GGA+U framework *Phys. Rev.* B **73** 195107

[46] Grimme S 2006 Semiempirical GGA-type density functional constructed with a long-range dispersion correction *J. Comput. Chem.* **27** 1787–99

[47] Heyd J, Scuseria G E and Ernzerhof M 2003 Hybrid functionals based on a screened Coulomb potential *J. Chem. Phys.* **118** 8207–15

[48] Heyd J, Scuseria G E and Ernzerhof M 2006 Erratum: 'Hybrid functionals based on a screened Coulomb potential' [J. Chem. Phys. 118, 8207 (2003)] *J. Chem. Phys.* **124** 219906

[49] Henderson T M, Paier J and Scuseria G E 2011 Accurate treatment of solids with the HSE screened hybrid *Phys. Status Solidi* B **248** 767–74

[50] Garcıa-Valdivia A A, Romero F J, Cepeda J, Morales D P, Casati N, Mota A J, Zotti L A, Palacios J J, Choquesillo-Lazarte D and Salmerón J F 2020 Rational design of an unusual 2D-MOF based on Cu (I) and 4-hydroxypyrimidine-5-carbonitrile as linker with conductive capabilities: a theoretical approach based on high-pressure XRD *Chem. Commun.* **56** 9473–6

[51] Blöchl P E 1994 Projector augmented-wave method *Phys. Rev.* B **50** 17953–79

[52] Kresse G and Joubert D 1999 From ultrasoft pseudopotentials to the projector augmented-wave method *Phys. Rev.* B **59** 1758–75

[53] Butler K T, Hendon C H and Walsh A 2014 Electronic chemical potentials of porous metal–organic frameworks *J. Am. Chem. Soc.* **136** 2703–6

[54] Frisch M J *et al* 2016 Gaussian 16 Rev. C.01 (Wallingford, CT)

[55] Johnston L L, Nettleman J H, Braverman M A, Sposato L K, Supkowski R M and LaDuca R L 2010 Copper benzenedicarboxylate coordination polymers incorporating a long-spanning neutral co-ligand: effect of anion inclusion and carboxylate pendant-arm length on topology and magnetism *Polyhedron* **29** 303–11

[56] Pang Y, Tian D, Zhu X-F, Luo Y-H, Zheng X and Zhang H 2011 Copper(II) and nickel(II) coordination polymers assembled from 2,4-dibenzoylisophthalic acid and different N-donor co-ligands: syntheses, crystal structures, and magnetic properties *CrystEngComm* **13** 5142–51

[57] Zhao J, Dong -W-W, Wu Y-P, Wang Y-N, Wang C, Li D-S and Zhang Q-C 2015 Two (3,6)-connected porous metal–organic frameworks based on linear trinuclear [Co$_3$(COO)$_6$] and paddlewheel dinuclear [Cu$_2$(COO)$_4$] SBUs: gas adsorption, photocatalytic behaviour, and magnetic properties *J. Mater. Chem.* A **3** 6962–9

[58] Rodríguez-Fortea A, Alemany P, Alvarez S and Ruiz E 2001 Exchange coupling in carboxylato-bridged dinuclear copper(II) compounds: a density functional study *Chem. Eur. J.* **7** 627–37

[59] Pakula R J and Berry J F 2018 Cobalt complexes of the chelating dicarboxylate ligand 'esp': a paddlewheel-type dimer and a heptanuclear coordination cluster *Dalton Trans.* **47** 13887–93

[60] Williams D E, Rietman J A, Maier J M, Tan R, Greytak A B, Smith M D, Krause J A and Shustova N B 2014 Energy transfer on demand: photoswitch-directed behavior of metal–porphyrin frameworks *J. Am. Chem. Soc.* **136** 11886–9

[61] Shannon R 1976 Revised effective ionic radii and systematic studies of interatomic distances in halides and chalcogenides *Acta Crystallogr.* A **32** 751–67

[62] Stavale F and Simmchen J 2018 Artificial photosynthesis inspired by PSII: water splitting on heterogeneous photocatalysts *Encyclopedia of Interfacial Chemistry* ed K Wandelt (Amsterdam: Elsevier) pp 327–33

[63] Yang R, Wang K, Long L, Xiao D, Yang X and Tan W 2002 A selective optode membrane for histidine based on fluorescence enhancement of meso−meso-linked porphyrin dimer *Anal. Chem.* **74** 1088–96

[64] Gulino A, Mineo P, Bazzano S, Vitalini D and Fragalà I 2005 Optical pH meter by means of a porphyrin monolayer covalently assembled on a molecularly engineered silica surface *Chem. Mater.* **17** 4043–5

[65] Di Natale C, Salimbeni D, Paolesse R, Macagnano A and D'Amico A 2000 Porphyrins-based opto-electronic nose for volatile compounds detection *Sensors Actuators* B **65** 220–6

[66] Hong Y H, Han J W, Jung J, Nakagawa T, Lee Y-M, Nam W and Fukuzumi S 2019 Photocatalytic oxygenation reactions with a cobalt porphyrin complex using water as an oxygen source and dioxygen as an oxidant *J. Am. Chem. Soc.* **141** 9155–9

[67] Call A, Cibian M, Yamamoto K, Nakazono T, Yamauchi K and Sakai K 2019 Highly efficient and selective photocatalytic CO$_2$ reduction to CO in water by a cobalt porphyrin molecular catalyst *ACS Catal.* **9** 4867–74

[68] Barkigia K M, Miura M, Thompson M A and Fajer J 1991 Models of photosynthetic chromophores: molecular structure of the bacteriochlorin (2,3,12,13-tetrahydro-5,10,15,20-tetraphenylporphinato)(pyridine)zinc(II) *Inorg. Chem.* **30** 2233–6

[69] Palma M, Cárdenas-Jirón G I and Menéndez Rodríguez M I 2008 Effect of chlorin structure on theoretical electronic absorption spectra and on the energy released by porphyrin-based photosensitizers *J. Phys. Chem.* A **112** 13574–83

[70] Lu K, He C and Lin W 2015 A chlorin-based nanoscale metal–organic framework for photodynamic therapy of colon cancers *J. Am. Chem. Soc.* **137** 7600–3

[71] Posligua V, Aziz A, Haver R, Peeks M D, Anderson H L and Grau-Crespo R 2018 Band structures of periodic porphyrin nanostructures *J. Phys. Chem.* C **122** 23790–8

[72] Marcus R A 1993 Electron transfer reactions in chemistry. Theory and experiment *Rev. Mod. Phys.* **65** 599–610

[73] Marcus R A 1956 On the theory of oxidation reduction reactions involving electron transfer I *J. Chem. Phys.* **24** 966–78